Electronic Supplementary Information for

Efficient and steady production of 1:2 syngas (CO/H_2) by simultaneously electrochemical reduction of CO_2 and H_2O

Wei Yang,[a,†] Ji-Hong Zhang,[a,†] Rui Si,[b] Li-Ming Cao,[a] Di-Chang Zhong[a,*] and Tong-Bu Lu[a]

[a] Institute for New Energy Materials and Low Carbon Technologies, School of Materials Science and Engineering, Tianjin University of Technology, Tianjin 300384, China. E-mail: dczhong@email.tjut.edu.cn (D. Zhong).

[b] Shanghai Synchrotron Radiation Facility, Shanghai Institute of Applied Physics, Chinese Academy of Sciences, Shanghai 201204, China.

[†] These authors contributed equally to this work.

Contents

1. Experimental details.

1.1 Materials:

All chemicals and materials were commercially obtained and used without any further purification. Solvents were dried and distilled for synthesis. Nafion solution (5 wt%) was purchased from Alfa Aesar. All solutions used in electrochemical experiments were prepared with Millipore water (18.2 MΩ). The purity of both Argon and CO_2 is 99.999%.

1.2 Synthesis:

The ligands **L^1, $[Co_2(OH)L^1](ClO_4)_3$, ZIF-8** were synthesized by literature methods [1-3].

L^1: (L^1= $(MX)_3(TREN)_2$), MX = m-xylyl groups, TREN= tris(2-aminoethyl)amine) A CH_3OH solution (150 mL) of tris(2-aminoethyl)amine (1.51 g, 0.0103 mol) was added dropwise to a stirred CH_3OH solution (300 mL) of benzene-1,3-dicarboxaldehyde (2.08 g, 0.0155 mol) over 1 h. After further stirred at room temperature for 24 h, the resulting yellowish solution was concentrated to 100 mL under reduced pressure. The solution was cooled to 0 °C on an ice bath, and $NaBH_4$ (4.30 g, 0.114 mol) was then added. The suspension was stirred at room temperature for 2 h, then heated to 50 °C and stirred at this temperature for an additional 20 h to ensure that the reduction was complete. The solvent was removed under reduced pressure, and water (50 mL) was added. The product was extracted with toluene. The organic phase was dried over Na_2SO_4 and filtered. Evaporation of the filtrate under reduced pressure yielded yellowish oil. It was recrystallized from toluene to give a white solid (2.16 g, 70%). To obtain the CO_2-free ligand, the dry product **L^1** was dissolved in a small amount of acetone, the solution was kept on an ice-bath, and excess $HClO_4$ was added dropwise to give a white precipitate. After the mixture was stirred for 15 min, the precipitate was filtered, washed with a small amount of acetone and diethyl ether, and then dried under vacuum to give the white solid **L^1**$\cdot 8HClO_4$

$[Co_2(OH)L^1](ClO_4)_3$: Under an argon atmosphere, an absolute ethanol solution (12 mL) of $Co(ClO_4)_2\cdot 6H_2O$ (2.07 g, 5.67 mmol) was added to an absolute ethanol solution (250 mL) containing **L^1**$\cdot 8HClO_4$ (3.00 g, 2.14 mmol) and NaOH (0.67 g, 16.80 mmol). The mixture was stirred at room temperature for 15 min. The resulted gray precipitate was filtered, washed with ethanol and diethyl ether, and dried under vacuum to give a gray powder (1.74 g, 75%).

Synthesis of ZIF-8: A MeOH solution (25 mL) of $Zn(NO_3)_2\cdot 6H_2O$ (950 mg, 5 mmol) was added slowly to a MeOH solution (25 mL) of 2-methylimidazole (2 g, 24.4 mmol)

with continuous stirring. The mixture was then kept undisturbed for 24 hours and ZIF-8 was obtained as precipitate. It was centrifuged and washed with DMF and MeOH repeatedly, and dried at 70 °C.

Table S1 The contents of Co and Zn in different catalysts measured by inductively coupled plasma-mass spectroscopy.

Catalysts	Co/%	Zn/%
5-Co_2L@ZIF-8-850	0.1332	14.63
10-Co_2L@ZIF-8-850	0.6419	6.051
20-Co_2L@ZIF-8-850	1.604	5.712
40-Co_2L@ZIF-8-850	2.498	5.192
10-Co_2L@ZIF-8-750	0.1965	22.13
10-Co_2L@ZIF-8-950	1.096	0.0287

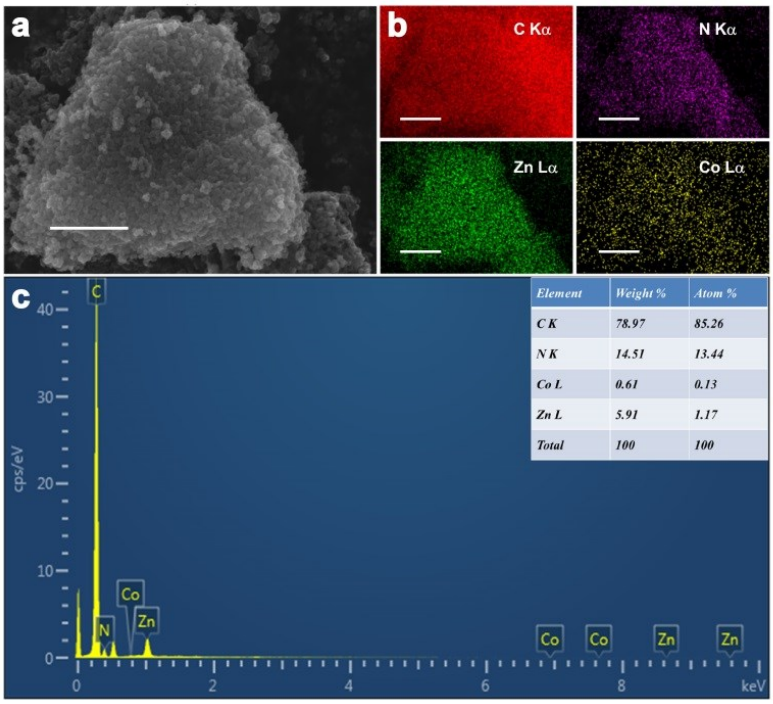

Fig. S1 Scanning electron microscopy (SEM) images (scale bar 2.5 μm) and energy-dispersive X-ray spectroscopy (EDS) elemental mapping of 10-Co_2L@ZIF-8-850.

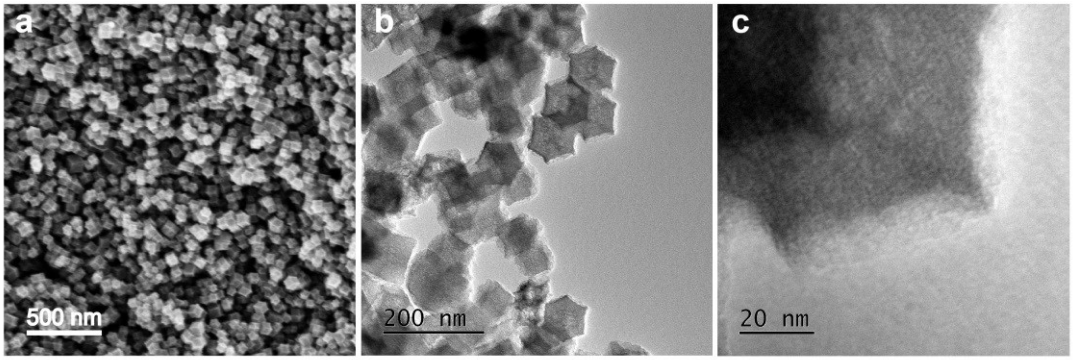

Fig. S2 (**a**) High resolution scanning electron microscopy (HRSEM) and (**b**, **c**) transmission electron microscopy (TEM) images of ZIF-8-850.

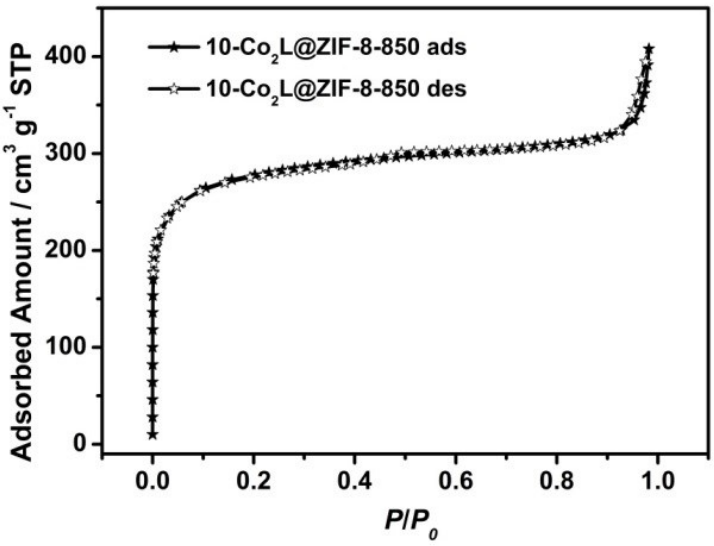

Fig. S3 N_2 sorption isotherms for 10-Co_2L@ZIF-8-850 at 77 K.

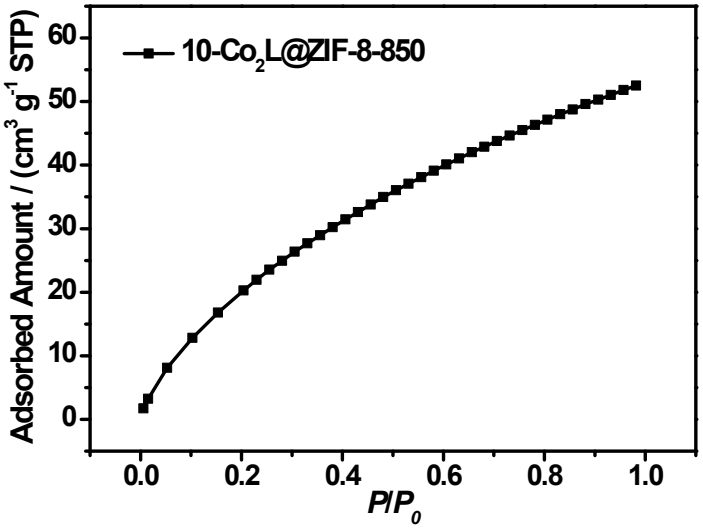

Fig. 4 CO_2 adsorption isotherm of 10-Co_2L@ZIF-8-850 at 298 K.

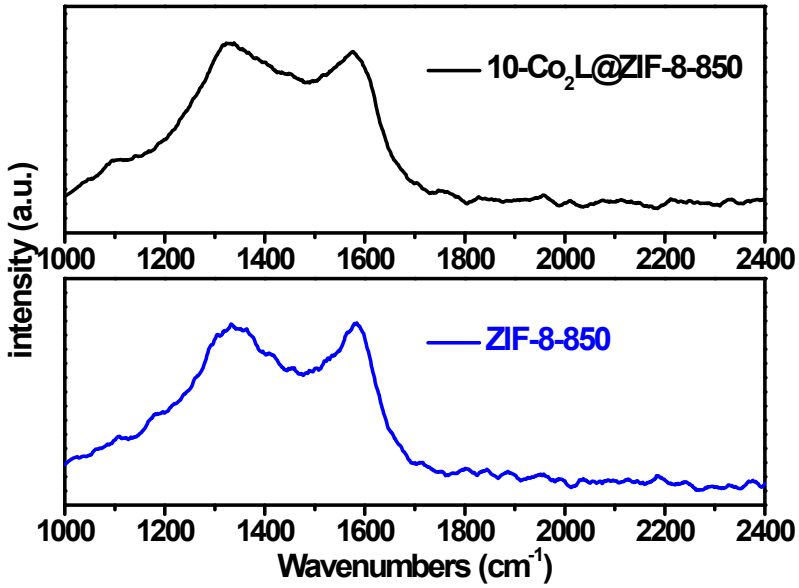

Fig. 5 Raman spectra of 10-Co_2L@ZIF-8-850 and ZIF-8-850.

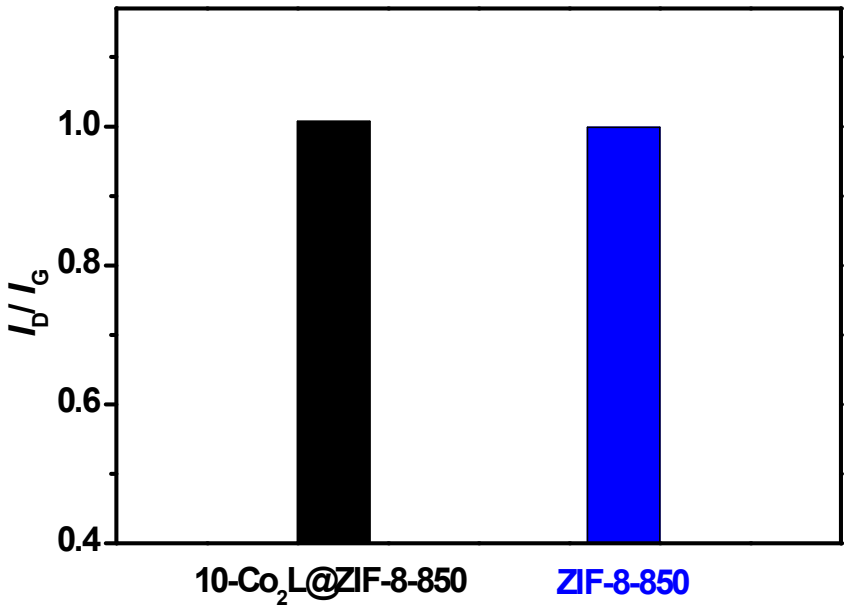

Fig. S6 Calculated I_G/I_D values for 10-Co_2L@ZIF-8-850 and ZIF-8-850.

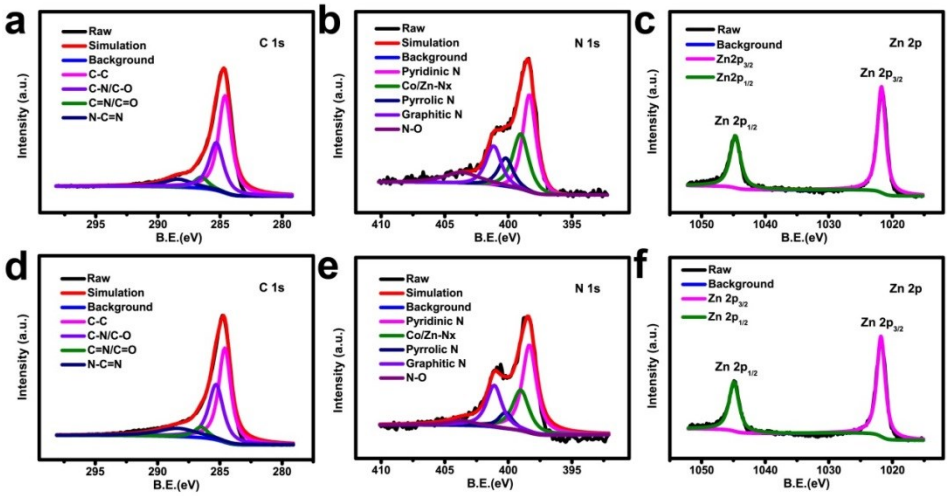

Fig. S7 C 1s, N 1s and Zn 2p high-resolution XPS spectra in 10-Co_2L@ZIF-8-850 (**a**, **b** and **c**, respectively), and ZIF-8-850 (**d**, **e** and **f**, respectively).

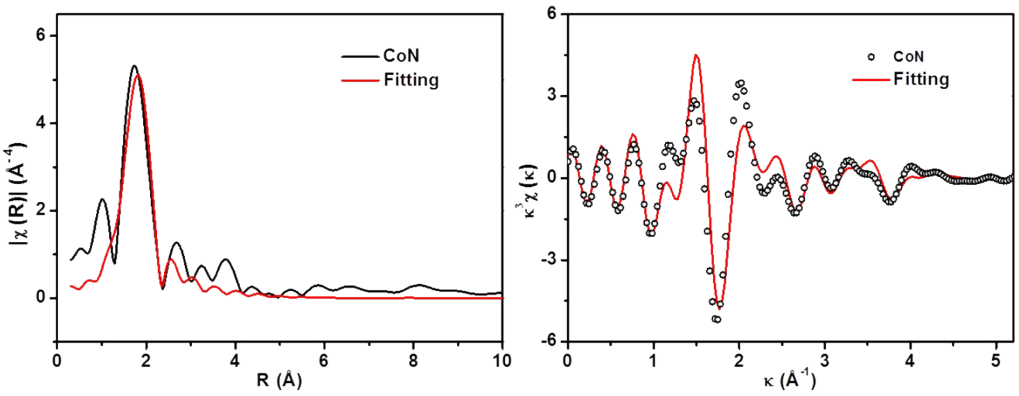

Fig. S8 Corresponding EXAFS fitting curves for 10-Co_2L@ZIF-8-850 at *k* space (Left) and *R* space (Right), respectively.

Table S2. Co K-edge EXAFS fitting results for 10-Co_2L@ZIF-8-850.

Sample	Co-C/N		σ^2(Å^2)	ΔE_0 (eV)
	R (Å)	*CN*		
10-Co_2L@ZIF-8-850	1.73±0.01	8.7±1.1	0.012±0.001	7.3±0.8

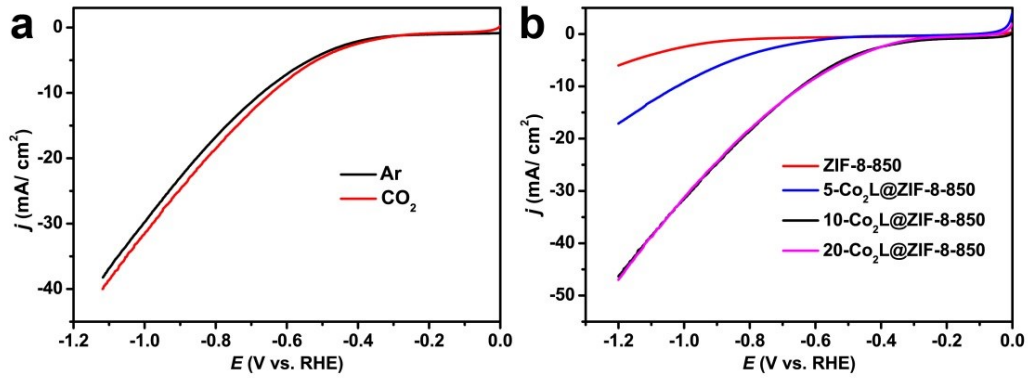

Fig. S9 (**a**) LSV curves of 10-Co_2L@ZIF-8-850 recorded in Ar- and CO_2-saturated 0.1 M $KHCO_3$ electrolyte. (**b**) LSV curves of *x*-Co_2L@ZIF-8-850 recorded in CO_2-saturated 0.1 M $KHCO_3$ electrolyte.

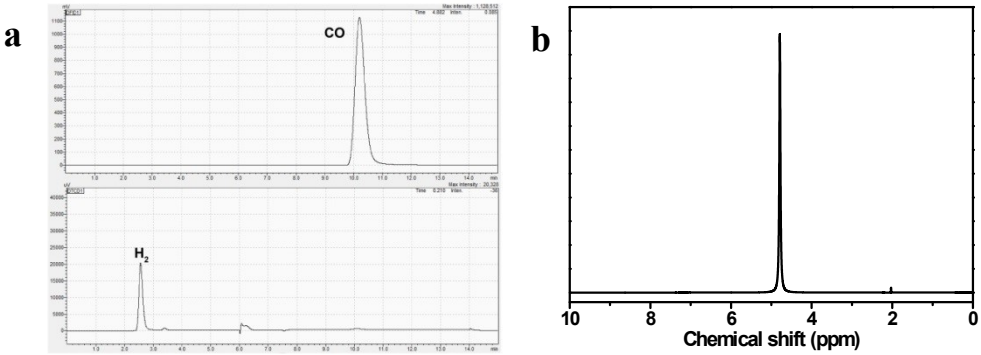

Fig. S10 (**a**) Gas chromatography (GC) and (**b**) ^{1}H NMR spectra of the electrolyte after electrolysis for 1 h in CO_2 atmosphere at -1.0 V by 10-Co_2L@ZIF-8-850, where the chemical shift at 4.76 corresponds to the H_2O.

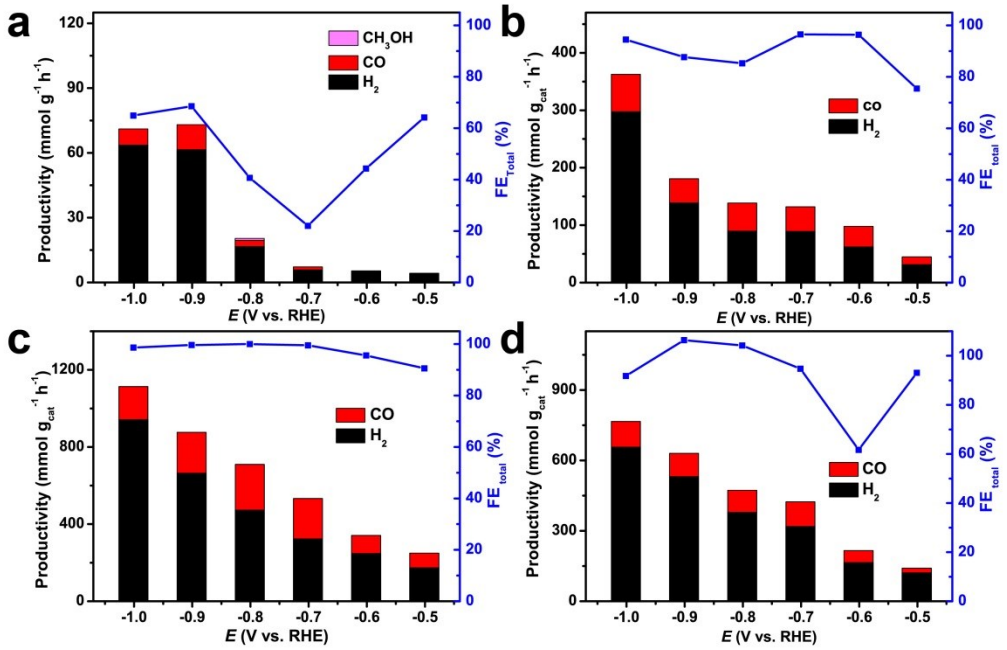

Fig. S11 The productivity (left Y-axis) and FE (right Y-axis) of (**a**) ZIF-8-850, (**b**) 5-Co_2L@ZIF-8-850, (**c**) 20-Co_2L@ZIF-8-850, (**d**) 40-Co_2L@ZIF-8-850) under different applied potentials, where the red and dark columns represent CO and H_2, respectively.

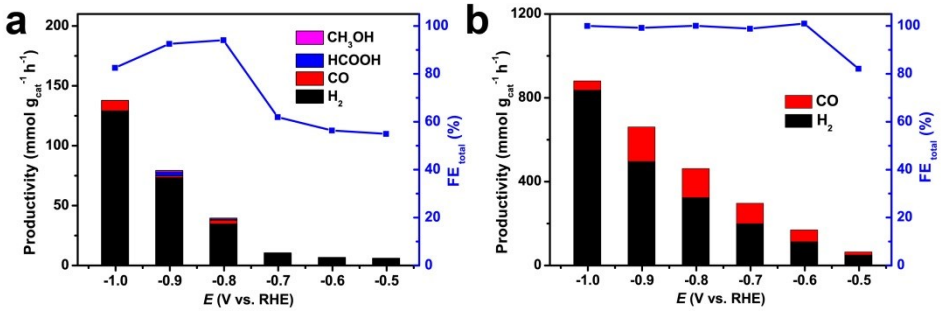

Fig. S12 The productivity (left Y-axis) and FE (right Y-axis) of (a) 10-Co_2L@ZIF-8-750 and (**b**) 10-Co_2L@ZIF-8-950 under different applied potentials, where the red and dark columns represent CO and H_2, respectively.

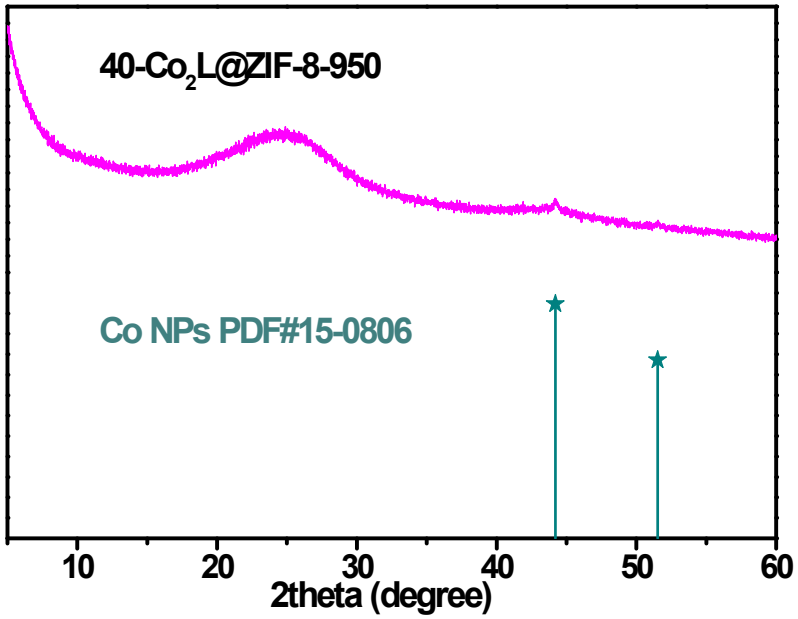

Fig. S13 Powder XRD pattern of 40-Co_2L@ZIF-8-850.

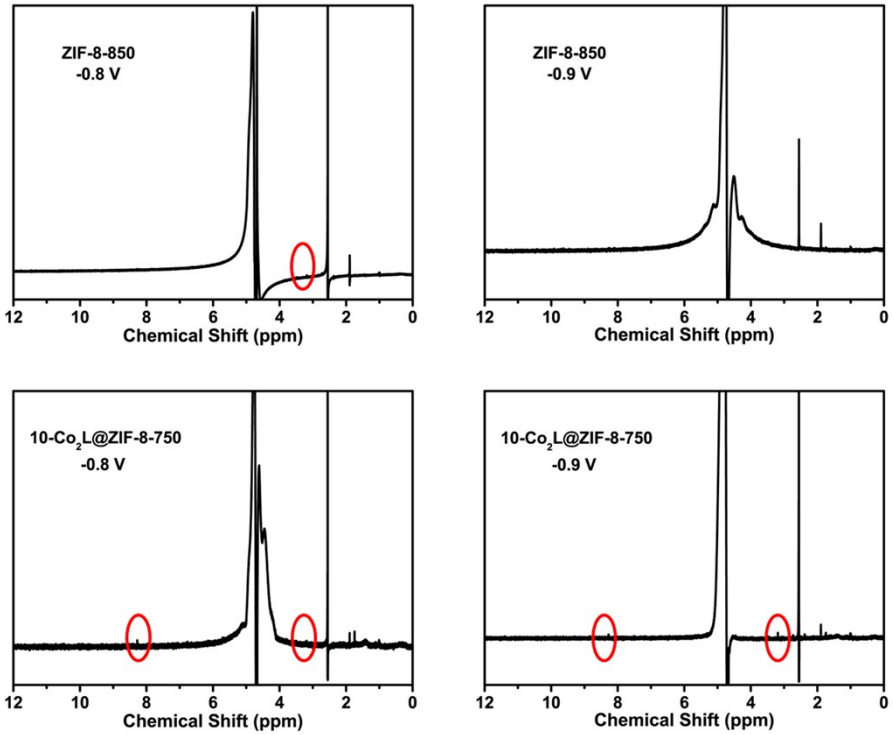

Fig. S14 ^{1}H NMR spectra of the electrolyte after electrolysis for 1 h in CO_2 atmosphere by ZIF-8-850 and 10-Co_2L@ZIF-8-750.

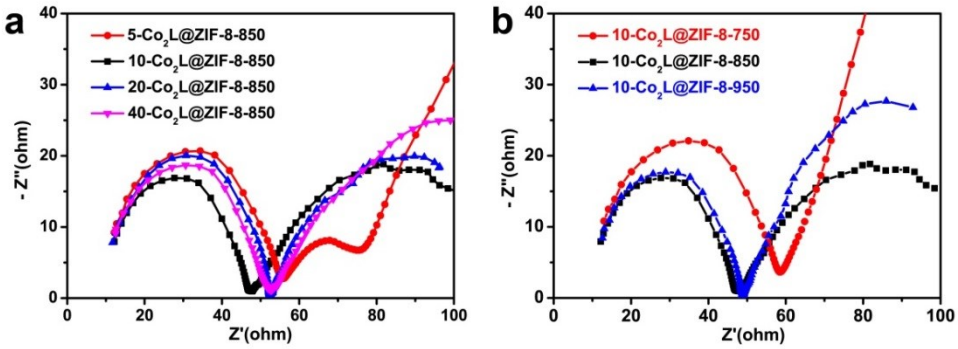

Fig. S15 The Nyquist plots of (**a**) *x*-Co_2L@ZIF-8-850 and (**b**) 10-Co_2L@ZIF-8-T, measured at -0.58 vs RHE.

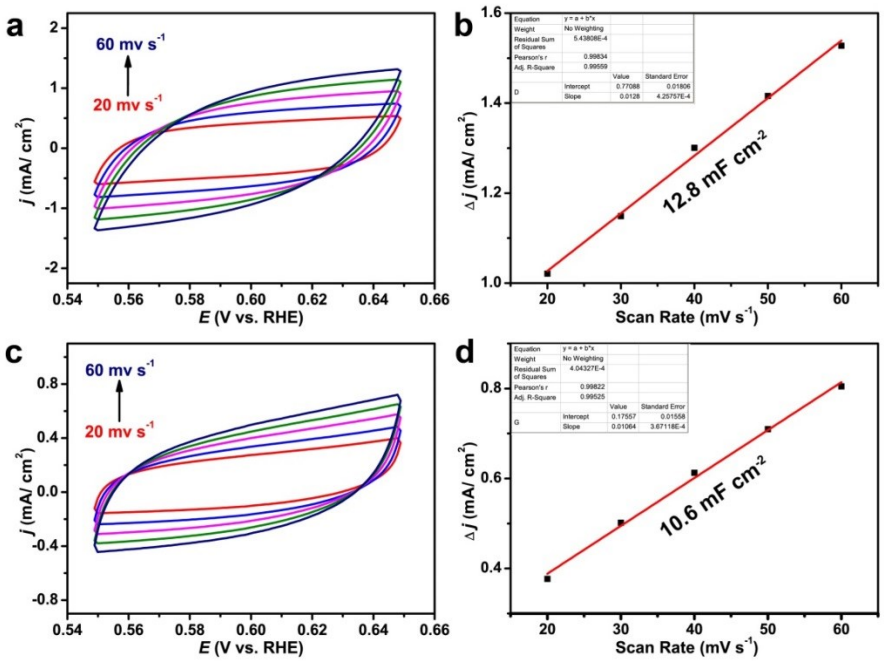

Fig. S16 (**a**) CV curves of 10-Co_2L@ZIF-8-850 at different scanning speeds in the range of 0.55-0.65 V vs. RHE. (**b**) The capacitive current density $\Delta j_{0.6\ V}$ as a function of scan rate for 10-Co_2L@ZIF-8-850. (**c**) CV curves of ZIF-8-850 at different scanning speeds in the range of 0.55-0.65 V vs. RHE. (**d**) The capacitive current density $\Delta j_{0.6\ V}$ as a function of scan rate for ZIF-8-850.

Table S3 Comparison of total current density (j_{total}) of various catalysts for CO_2 electroreduction to 1:2 CO/H_2 syngas.

Catalysts	j (mA/cm^2)	Potential (V vs. RHE)	Electrolyte	CO/H_2	Refs.
10-Co_2L@ZIF-8-850	31.7	-1.0	0.1 M $KHCO_3$	1:2:	This work
Ag Nanowires	<3	−0.8 to −1.3	0.5 M $KHCO_3$	1:4 to 1:1	[5]
20% wt Ag/g–C_3N_4	4.7~7.6	-1.05 to -1.15	0.1 M KH_2PO_4/K_2HPO_4 buffer	1:2	[6]
Pd/C	0.15	-0.5	0.5M $NaHCO_3$	1:2	[7]
Core–shell Cu/Au	~14.0	-0.65	0.5 M $KHCO_3$	1:2	[8]
$CdS_{0.22}Se_{0.78}$	26.5	-1.2	0.1 M $KHCO_3$	1:1 1:2	[9]
2/3 CuUPD	~20	-0.65	0.5 M $KHCO_3$	1:1	[10]
Co_3O_4–CDots–C_3N_4	< 0.25 5.78	−0.4 −0.75	0.5 M $KHCO_3$	1:2 1:1	[11]
Zn–1	~26.3	−1.0	0.1 M $KHCO_3$	1:1	[12]
CoSA-HNC	~14	−1.0	0.1 M $KHCO_3$	1:2	[13]
Ag-SnS_2	15.5	−1.0	0.5 M $KHCO_3$	1:1	[14]

References

1. J. M. Chen, W. Wei, X. L. Feng and T. B. Lu, CO_2 fixation and transformation by a dinuclear copper cryptate under acidic conditions, *Chem. Asian J*, 2007, **2**, 710-719.
2. T. Ouyang, H. H. Huang, J. W. Wang, D. C. Zhong and T. B. Lu, A Dinuclear Cobalt Cryptate as a Homogeneous Photocatalyst for Highly Selective and Efficient Visible-Light Driven CO_2 Reduction to CO in CH_3CN/H_2O Solution, *Angew. Chem. Int. Ed.*, 2017, **129**, 756-761.
3. S. Mukhopadhyay, J. Debgupta, C. Singh, A. Kar and S. K. Das, A Keggin Polyoxometalate Shows Water Oxidation Activity at Neutral pH: POM@ZIF-8, an Efficient and Robust Electrocatalyst, *Angew. Chem. Int. Ed.*, 2018, **57**, 1918-1923.
4. K. Jiang, G. Chen and H. Wang, Synthesis and Performance Characterizations of Transition Metal Single Atom Catalyst for Electrochemical CO_2 Reduction, *Joule*, 2018, **3**, 1-11.
5. W. Xi, R. Ma, H. Wang, Z. Gao, W. Zhang and Y. Zhao, Ultrathin Ag Nanowires Electrode for Electrochemical Syngas Production from Carbon Dioxide, *ACS Sustain. Chem. Eng.*, 2018, **6**, 7687-7694.
6. F. Sastre, M. J. Muñoz-Batista, A. Kubacka, M. Fernández-García, W. A. Smith, F. Kapteijn, M. Makkee and J. Gascon, Efficient Electrochemical Production of Syngas from CO_2 and H_2O by using a Nanostructured $Ag/g\text{-}C_3N_4$ Catalyst, *ChemElectroChem*, 2016, **3**, 1497-1502.
7. W. Sheng, S. Kattel, S. Yao, B. Yan, Z. Liang, C. J. Hawxhurst, Q. Wu and J. G. Chen, Electrochemical reduction of CO_2 to synthesis gas with controlled CO/H_2 ratios, *Energy Environ. Sci*, 2017, **10**, 1180-1185.
8. K. Chen, X. Zhang, T. Williams, L. Bourgeois and D. R. MacFarlane, Electrochemical reduction of CO_2 on core-shell Cu/Au nanostructure arrays for syngas production, *Electrochimica Acta*, 2017, **239**, 84-89.
9. R. He, A. Zhang, Y. Ding, T. Kong, Q. Xiao, H. Li, Y. Liu and J. Zeng, Achieving the Widest Range of Syngas Proportions at High Current Density over Cadmium Sulfoselenide Nanorods in CO_2 Electroreduction, *Adv Mater*, 2018, **30**, 1705872.

10. M. B. Ross, C. T. Dinh, Y. Li, D. Kim, P. De Luna, E. H. Sargent and P. Yang, Tunable Cu Enrichment Enables Designer Syngas Electrosynthesis from CO_2, *J. Am. Chem. Soc.*, 2017, **139**, 9359-9363.
11. S. Guo, S. Zhao, X. Wu, H. Li, Y. Zhou, C. Zhu, N. Yang, X. Jiang, J. Gao, L. Bai, Y. Liu, Y. Lifshitz, S. T. Lee and Z. Kang, ACo_3O_4-CDots-C_3N_4 three component electrocatalyst design concept for efficient and tunable CO_2 reduction to syngas, *Nat. Commun.*, 2017, **8**, 1828.
12. B. Qin, Y. Li, H. Fu, H. Wang, S. Chen, Z. Liu and F. Peng, Electrochemical Reduction of CO_2 into Tunable Syngas Production by Regulating the Crystal Facets of Earth-Abundant Zn Catalyst, *ACS Appl. Mater. Interfaces*, 2018, **10**, 20530-20539.
13. X. Song, H. Zhang, Y. Yang, B. Zhang, M. Zuo, X. Cao, J. Sun, C. Lin, X. Li and Z. Jiang, Bifunctional Nitrogen and Cobalt Codoped Hollow Carbon for Electrochemical Syngas Production, *Adv. Sci.*, 2018, **5**, 1800177.
14. R. He, X. Yuan, P. Shao, T. Duan and W. Zhu, Hybridization of Defective Tin Disulfide Nanosheets and Silver Nanowires Enables Efficient Electrochemical Reduction of CO_2 into Formate and Syngas, *Small*, 2019, **15**, 1904882.